Proceedings of the 39th IAHR World Congress
19–24 June 2022, Granada, Spain
doi://10.3850/IAHR-39WC2521716X2022930

Understanding the Influences of Large-scale Atmospheric and Oceanic Circulations on the Snow-cover of a Himalayan Basin

Shairik Sengupta [1], Rajarshi Das Bhowmik [2]

[1,2] Indian Institute of Science, Bengaluru, India
shairiks@iisc.ac.in
rajarshidb@iisc.ac.in

Abstract

Himalayan basins have great hydropower potential. In recent years, several of Himalayan basins have experienced flood conditions attributed to anthropogenic climate change and changes in land use. Therefore, there is a growing interest in issuing season-ahead flow forecasts based on atmospheric and oceanic teleconnections. The current study is a preliminary step towards developing a sub-seasonal-to-seasonal flow forecast model. The study investigates potential drivers of river flow at different time-lags. It is noted that an efficient prediction of the snow cover would lead to a skillful flow forecast. Therefore, the study estimates the correlation coefficients between ten climate indices and snow cover, and subsequently snow cover and river discharge at a downstream outlet of the Upper Bias River basin. Results confirm that a statistically significant correlation exists between climate indices and snow cover. Additionally, a linear regression model between snow cover and river discharge is developed to understand the linear dependence between the two variables.

Keywords: Teleconnections; Snow cover; Himalayan River Basin; Streamflow forecasts; Hydroclimate

1. INTRODUCTION

In recent years Indian Himalayas have witnessed major flooding events Shah et al., 2018). Former studies have indicated that global climate change is impacting Himalayan glaciers and snow cover. This has resulted in flash floods, landslides, and debris flow. The region substantially influences the downstream, and low elevation population as glacier and snow-fed rivers such as the Ganges, Indus originate in the Himalayas. Despite the recurring natural disasters in the region, Himalayan rivers have a great potential for hydropower generation (Sharma and Kuniyal, 2016). Considering these, it is of significant interest to develop short-term to long-term operational planning to manage the water resource efficiently. An essential component of operational planning is skillful sub-seasonal to seasonal (S2S) forecast. The current study investigates the potential to develop a skillful S2S forecast for the upper Beas River basin.

The first task in developing a S2S forecast system to predict streamflow is to identify the drivers that influence streamflow. Kumar (2007) reported that Himalayan rivers maintain baseflow from the glacial meltwater, and the river discharge experiences strong seasonality. Hussain (2021) found that snow cover variability needs to be addressed first to predict streamflow. In recent years Chandel and Ghosh (2021) and Laha et al. (2021) found that glacier melt and seasonal snowmelt are major drivers for long-term simulation of streamflow at a downstream location. Hence the current study hypothesizes that to predict the season ahead streamflow the snow-covered needs to be predicted first. Teleconnections between large oceanic and atmospheric circulations and hydrometeorological variables have been widely investigated by former studies. Shaman (2005) reported that Himalayan snow cover has been influenced by the El-Nino and the Southern Oscillation. Other teleconnections such as the North Atlantic Oscillations (NAO) and the Pacific decadal oscillations (PDO) also have shown their influence on Himalayan precipitation (Singh et al. 2009 and Chen et al. 2020). Arctic Oscillation (AO) and Quasi-biennial Oscillation (QBO) have traditionally influenced the snow cover. However, studies on their influence on Indian Himalayas by Bamzai (2003) and Peings et al. (2017) have been limited to effects on temperature and rainfall. Considering this, a comprehensive analysis is required to identify the teleconnections between atmospheric-oceanic teleconnections at an appropriate spatial and temporal scale.

A skillful season ahead prediction of snow cover would potentially assess a skillful season ahead forecast of streamflow. The season ahead flow forecasts are typically issued by statistical models as atmospheric uncertainty is large beyond 3-7 days (Chow, 2017). Earlier studies have considered parametric to non-parametric statistical models to issue season ahead streamflow forecasts. Such models traditionally consider Sea Surface Temperature (SST) forecasts as model predictors. However, limited efforts have been

made to issue season ahead forecasts in snow-dominated and glacierized basins. Considering this, the study has two objectives, as given below.

1. Identify the effects of climate teleconnections on snow cover
2. use snow cover to predict streamflow.

2. STUDY AREA

The present study considers the upper reaches of the Beas basin (Figure 1). The Beas originates from glaciers in the western Himalayas, in the Indian state of Himachal Pradesh. We consider the delineated catchment upstream of Pandoh, where a major dam was constructed in 1977 for hydroelectric power generation. Our study area spans about 5337 square kilometers. The river starts from Beas Kund, a lake 3681meters above sea level in the Pir-Panjal range. From Beas Kund to Pandoh, the river travels 116 kilometers. About 371 square kilometers of the basin are covered by approximately 236 glaciers (Dutta et al., 2012).

Another 409 square kilometers remain under snow cover (Li et al., 2019). Snow cover in the area develops from November, peaks between January to February, and starts retreating by April. The climate in the area is varied due to the altitude variation involved – high peaks are located above 6000 meters, while the lowest point is around 694 meters above sea level. Summer temperatures rise to 20°C, whereas winter temperatures can fall below 2°C. Precipitation has an annual average of 122 cm, two-thirds of which is contributed by the monsoon. The study divides the basin into two regions based on high and low elevations (Figure 2). The high elevation region has elevations from 3949m to 6258 m, whereas the low elevation region ranges from 694 m to 3949 m. A k-means clustering based on altitude is used to identify two regions.

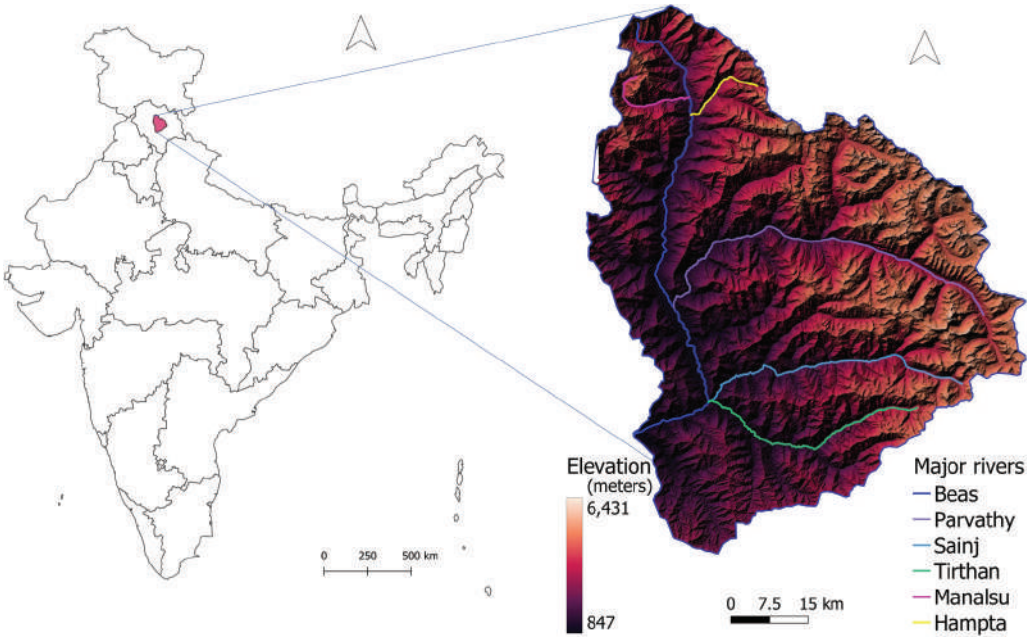

Figure 1. Beas Basin (overlaid on an elevation map), the Beas River and its major tributaries with its location in India.

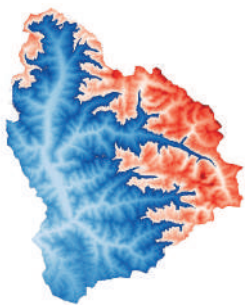

Figure 2. Basin in divided in to two regions based on high and low elevations. A k-means clustering is applied to separate the two zones. Blue color represents the low elevation region, while the red represents the high elevation region.

3. DATA

Elevation data used by the current study is obtained from the Shuttle Radar Topography Mission (SRTM) with a 30 meters resolution. The study considers Land Sat 8 images of the study area for April 2013 to August 2021 at 30 meters resolution. Land Sat 8 images are available at 16-day time steps. These images are subsequently averaged to arrive at a monthly resolution. Both these datasets are downloaded from the Earth Explorer web interface, hosted by the U. S. Geological Survey.

Daily river discharge data at the outlet location (upstream of Pandoh) is obtained from the GLOFAS-ERA5 system, developed by Harrigan et al. (2020). Daily discharge data were converted to monthly average discharges.

Oceanic and atmospheric indices at monthly time steps are obtained (May 2012 to August 2021). Details regarding the climate indices are provided in Table 1.

Table 1. Climate indices and data source.

Phenomenon	Measured Variable	Index	Source
El-Nino Southern Oscillation	Sea Surface Temperature	NINO indices (NINO 1+2, NINO 3, NINO3.4, NION4)	Lamont-Doherty Earth Observatory
Quasi-Biennial Oscillation	Vertical Wind Profile	QBO	Lamont-Doherty Earth Observatory
Indian Ocean Dipole	Sea Surface Temperature	Dipole Mode Index (DMI)	National Oceanic and Atmospheric Administration
Pacific Decadal Oscillation	Sea Surface Temperature	PDO	National Oceanic and Atmospheric Administration
Arctic Oscillation	Air pressure	AO	National Oceanic and Atmospheric Administration
North Atlantic Oscillation	Air pressure	NAO	National Oceanic and Atmospheric Administration
El-Nino southern Oscillation	Air pressure	Southern Oscillation Index (SOI)	National Oceanic and Atmospheric Administration

4. METHODS

The analysis follows three major steps:

1.An analysis of snow cover

2.A principal component analysis (PCA) to identify the pixels contributing to seasonal snow variability

3.Correlation analysis to understand the dependence between teleconnection, snow, and river discharge

4.1. Analysis of Snow Cover

The Land Sat images are screened for cloud cover; following which, NDSI is calculated for each image, using equation 1. NDSI is estimated using the Green (0.53μm -0.59 μm) and SWIR1 (1.57 μm -1.65 μm) bands of Land Sat images.

$$NDSI = \frac{GREEN - SWIR}{GREEN + SWIR} \quad [1]$$

NDSI is constructed using the property of snow being highly reflective in the visible range while being absorptive in the short wave infra-red region of the electromagnetic spectrum. As cloud cover is pre-eliminated, non-zero positive values of NDSI correspond to the amount of snow present in a 30m-by-30m grid corresponding to each pixel. Negative NDSI values were replaced with zero, as zero and negative NDSI values indicate the absence of snow. The study obtains three representatives of snow cover estimates

1.NDSI value at each pixel,

2.ii) fractional snow-covered area (equation 2)

3.iii) fractional area covered in temporary snow (equation 3).

In equation 3, the area under permanent snow cover is estimated by summing up the pixels where NDSI values remain non-zero for an entire season or an entire year. Therefore, the metric in equation 3 represents the intra-seasonal or intra-annual variation in the area covered in temporary snow.

$$Fractional\ snow\ covered\ area = \frac{Area\ under\ snow\ cover\ (NDSI>0)}{Area\ of\ the\ Basin} \quad [2]$$

$$Fractional\ area\ covered\ in\ temporary\ snow = \frac{Snow\ covered\ area - Area\ under\ permanent\ snow\ cover(entire\ year\ or\ season, as\ required)}{Area\ of\ the\ Basin} \quad [3]$$

4.2 Principal Component Analysis

Principal component analysis is a dimension-reduction approach that applies a linear transformation to variables. Principal components share useful information related to spatio-temporal variability. Principal components are uncorrelated to each other. A principal component analysis was applied on NDSI datasets, i.e., NDSI time-series for each pixel. The first component (PC1) explains the maximum of the total variance of the NDSI dataset; the second component (PC2) explains the maximum of the remaining variance, and so on. Further, the coefficients of PCs (also known as loadings) indicate the grid points contributing to the spatio-temporal variability in the NDSI data. The study retains only a few PCs for further analysis, thus reducing the large number of pixels covering the basin which, otherwise, would have been translated to a large set of predictands. PC analysis is either applied on NDSI values covering the entire basin or NDSI values for high/low elevation regions.

4.3 Correlation Analysis

The study estimated linear and non-linear correlation between principal components of NDSI values across pixels and the climate indices. Pearson correlation coefficient estimates the linear dependence, whereas Kendall's Tau measures non-linear dependence. Additionally, the study investigates the dependence between snow cover (from equations 2 and 3) and climate indices. To develop a comprehensive understanding of the influence of teleconnections on snow, the study considers lagged predictors to estimate the correlations. For example, a linear correlation between the first principal component at time step t and the PDO at time step t-4 would indicate that PDO influences the values of PC of NDSI four months later.

Similarly, the linear and non-linear relationships between principal components of NDSI values across pixels and river discharge were also explored. The same experiment was conducted with the fractional snow-covered area and fractional temporary snow-covered area as predictors of river discharge. These were done for various leads of river discharge. For example, a linear correlation between snow cover at time step t, and river discharge at t + 2 would indicate snow cover affects river discharge of two months later.

5. RESULTS

The study estimates the monthly mean of NDSI values for each pixel to understand the seasonality in snow cover over the basin (Figure 3). High amounts of snow spread over a large part of the basin are witnessed during winter. In summer, snowmelt starts; hence NDSI values are lower than in winter. Also, during summer, the snow-covered area recedes to higher altitudes. The lowest snow (with respect to both amount and area) is observed in the monsoon. In fall, snow cover starts to develop again, to attain the peak in the winter. Due to the strong seasonal character, for subsequent analysis, the time series was separated into four seasons: Winter (December, January, February), Summer (March, April, May), Monsoon (June, July, August, September), and Fall (October, November). Further, the variability in NDSI suggests a substantial difference in snow covers depending on altitude, which validates the previous classification of high and low elevation regions.

Results related to the PCA on NDSI datasets are presented in Figures 4 and 5. Figure 4 shows the variance explained by the first three principal components for four seasons over the whole basin (4a), high elevation region (4b), and low elevation region (4c). The loadings of the first Principal Components of the high elevation region and low elevation region are given in Figure 5(a). Loadings obtained from conducting PCA over the whole basin are shown in Figure5(b). The PCA analysis confirms that the first PC explains approximately 50% of the total variance. The first three PCs explain 70% of the total variance. The study found that pixels in high mountain valleys receive higher loadings than the low elevation region, indicating higher spatiotemporal variability in NDSI at high altitude valleys. The current study considers the first two PCs for further analysis.

The study investigates major drivers of the NDSI principal components at different time-lags for four seasons. In Figure 6, subplots (a) to (d) are related to a correlation analysis when principal components are

estimated using NDSI values for the entire basin. Subplots (6e) to (6h) and subplots (6i) to (6j) are related to a correlation analysis when principal components are estimated using NDSI values for the low elevation region and the high elevation region, respectively.

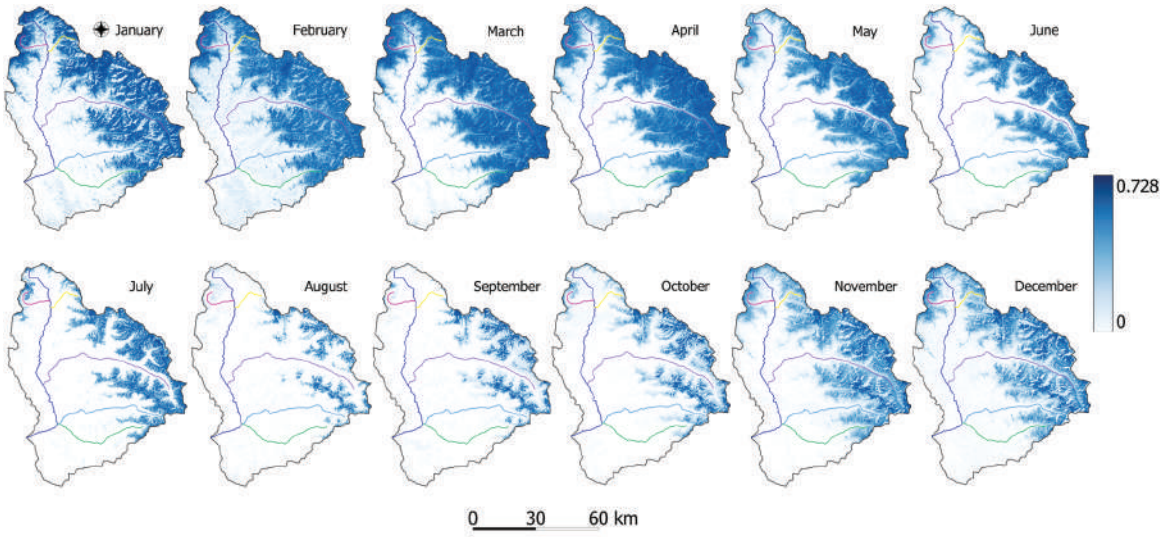

Figure 3. NDSI at each pixel averaged over each month, for all observations. High NDSI values are darker blue, and 0 is shown as white. The river network is overlaid for reference.

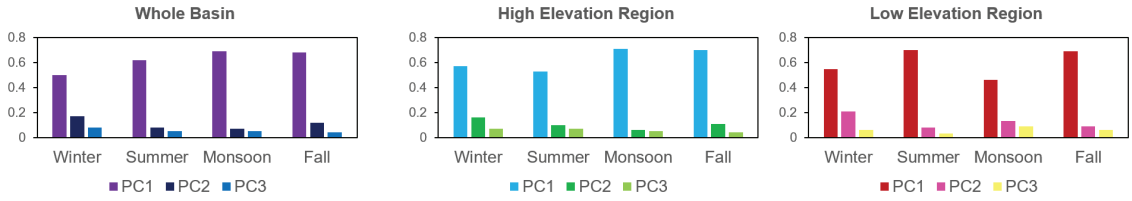

Figure 4. Proportion of variance for the first three principal components (PC) related to different elevation regions and seasons.

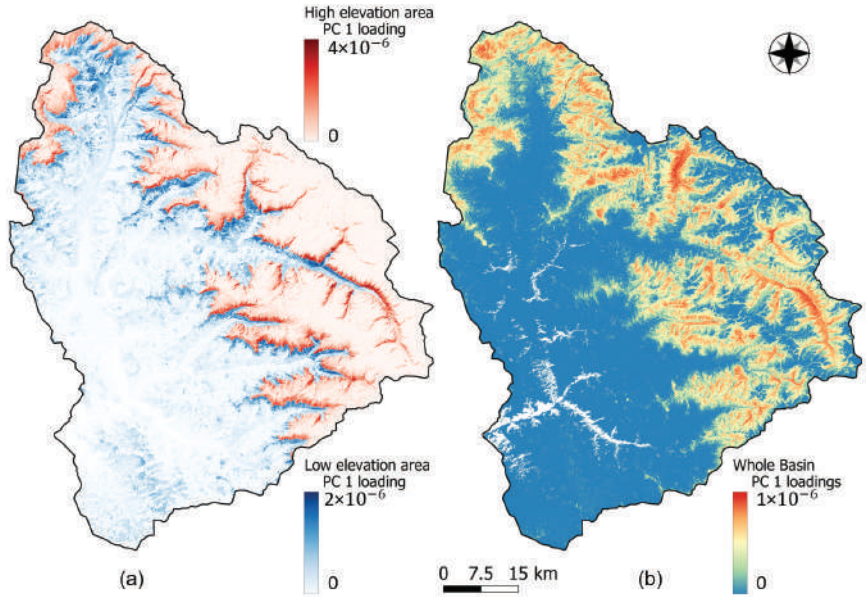

Figure 5. Loadings (rotations) of the first principal components at each point of high elevation area (red) and low elevation area (blue) – figure (a), and whole basin (blue to red) – figure (b).

The major drivers have been plotted only if the corresponding correlation value is statistically significant at a given time lag. Statistical significance is estimated using the formula $\pm 1.96/\sqrt{(n-3)}$, where n denotes the number of observations. The study found that major drivers for the whole basin are present at different lags for the fall season. During winter, statistically significant drivers are noted at 8-, 9-, and 11-month lags. In the low elevation, fall and winter seasons exhibit a higher number of drivers than the summer and the monsoon. Whereas in the high elevation, DMI yields a strong correlation at lag 1, but major drivers are higher in number during the fall as compared to other seasons.

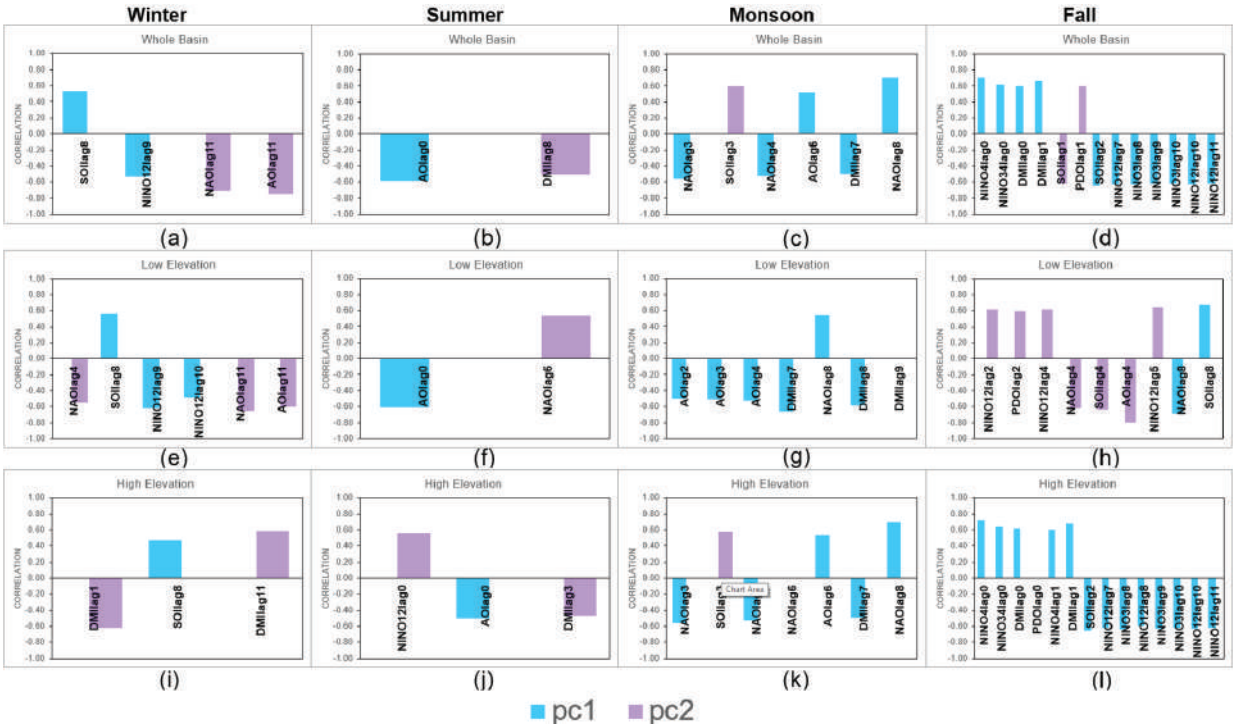

Figure 6. Correlation between PCs of NDSI and climate indices.

A similar analysis is performed to identify the predictor of fractional snow-covered area (subplots 7a to 7d) and fractional temporary snow-covered area (subplots 7e to 7h). The study found that a greater number of drivers for the fractional snow-covered area are available in the fall compared to other seasons. However, more drivers for the fractional temporary snow-covered area are available during the winter compared to other seasons. The analysis clearly shows the advantage of dividing the basin into two regions as the influence of climate indices significantly depends on the elevation.

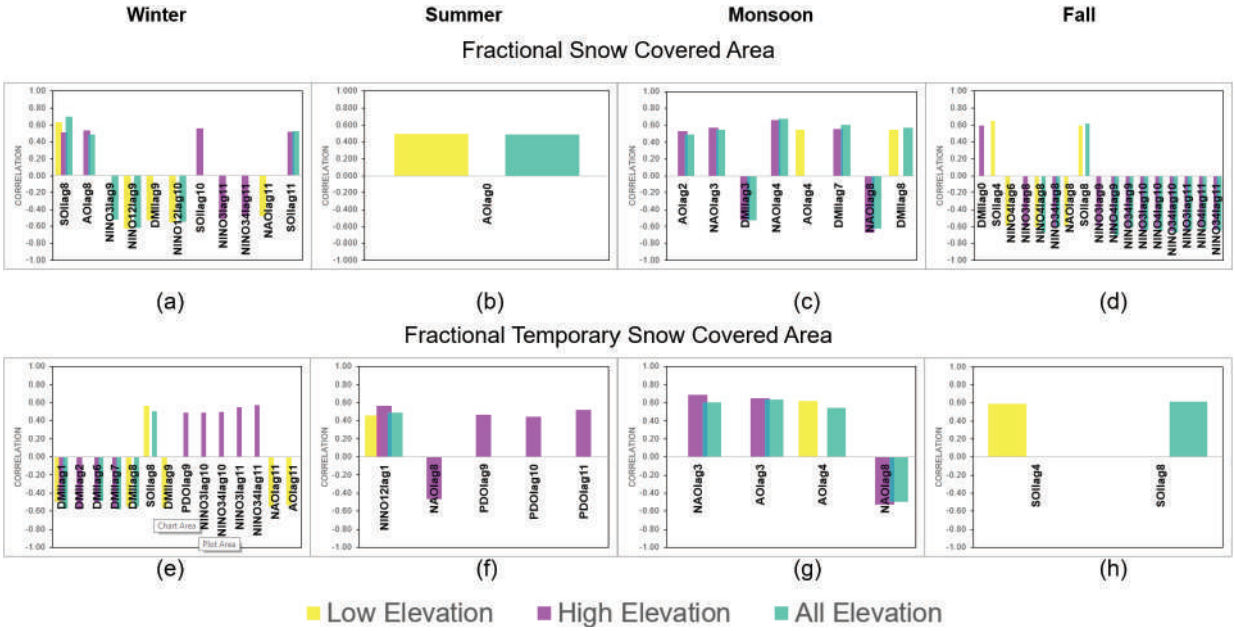

Figure 7. Correlation between snow-covered areas and climate indices.

Finally, the study develops regression relationships between potential lagged predictors and river discharges. Representative results are presented in Figure 8(a - d) for winter, summer, monsoon, and fall, respectively, where the discharge is predicted months ahead using the fractional snow cover and principal components of NDSI values. Results confirm that months-ahead discharge prediction has great potential, but the overall skill of linear models depend on the operating driver, the lag, the season, and the average altitude of the region.

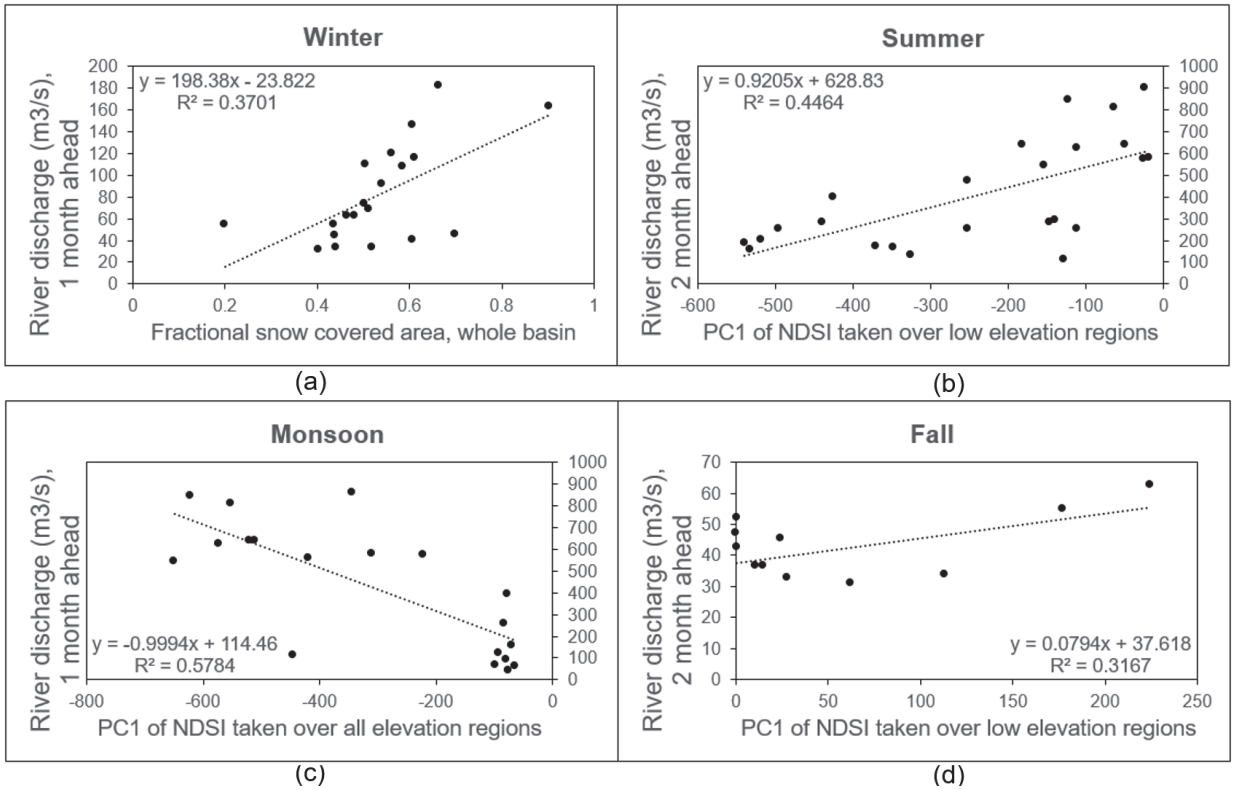

Figure 8. regression relationship between river discharge and snow representatives (PC of NDSI or fractional snow cover area)

6. SUMMARY AND DISCUSSION

The present study establishes that climate indices can be used to predict snow cover in the Beas Basin, using which water discharge can be estimated at a season ahead. Significant findings of the study are as follows. In winter, various climate teleconnections affect the amount of snow – an effect most pronounced in low elevation regions. This is likely as snow amount in higher altitudes is primarily dependent on the altitude–temperature relation. The fractional area of the basin covered in snow is found to be a potential predictor of river discharge. A positive correlation between snow cover and river discharge exists: as the snow cover increases the snowmelt potential also increases. During summer, a lower number of potential climate drivers of snow cover are found as local precipitation plays a crucial role. The first Principal Component of NDSI over low elevation regions is found to be a potential driver of river discharge in summer. In monsoon, the first Principal Component of NDSI over the entire basin has a strong influence on the streamflow. During fall, potential climate drivers at higher lags are found. The first Principal Component of NDSI over the low elevation regions controls the river discharge. The NINO indices typically exhibit a negative correlation with the snow-covered area, and a positive correlation with temporary snow cover, indicating strong ENSO signals result in a lesser amount of snow. Overall, the current study provides a groundwork to understand the influence of large-scale atmospheric and oceanic circulations on the snow cover for a representative Himalayan Basin. The study concludes that teleconnections have the potential to predict river discharge at the season ahead; however, further analysis is required to provide a comprehensive analysis.

7. REFERENCES

AO: National Weather Service – Climate Prediction Center, National Oceanic and Atmospheric Administration. (nd). *Arctic Oscillation (AO).* https://www.cpc.ncep.noaa.gov/products/precip/CWlink/daily_ao_index/ao.shtml.

Bamzai, A. (2003). Relationship between snow cover variability and Arctic oscillation index on a hierarchy of time scales. *International Journal of Climatology*, 23, 131-142.

Chandel, V.S., Ghosh, S. (2021). Components of Himalayan River Flows in a Changing Climate. *Water Resources Research,* 57(2).

Chen, Y., Duan, A. and Li, D. (2020). Connection between winter Arctic Sea ice and west Tibetan Plateau snow depth through the NAO. *International Journal of Climatology*. 41(5), 846-861.

Chow, V.T., Maidment, D., Mays, L. (2017). *Applied Hydrology.* McGraw Hill Education.

DMI: Global Climate Observing System - Working Group on Surface Pressure. (nd). *Dipole Mode Index (DMI).* https://psl.noaa.gov/gcos_wgsp/Timeseries/DMI/.

Dutta, S., Ramanathan, A.L. and Linda, A. (2012). Glacier fluctuation using Satellite Data in Beas basin, 1972–2006, Himachal Pradesh, India. *Journal of Earth System Sciences*, 121, 1105–1112.

Harrigan, S., Zsoter, E., Alfieri L. et al. (2020). GloFAS-ERA5 operational global river discharge reanalysis 1979–present. *Earth System Science Data,* 12(3), 2043–2060.

Hussain, A., Cao, J., Hussain, I., Begum, S., Akhtar, M., Wu, X., Guan, Y. and Zhou, J. (2021). Observed trends and variability of temperature and precipitation and their global teleconnections in the Upper Indus Basin, Hindukush-Karakoram-Himalaya. *Atmosphere*, 12(8), 973.

Kumar, V., Singh, P. and Singh, V. (2007) Snow and glacier melt contribution in the Beas River at Pandoh Dam, Himachal Pradesh, India, *Hydrological Sciences Journal*, 52(2), 376-388.

Laha, S., Banerjee, A., et al. (2021). The control of climate sensitivity on variability and change of summer runoff from two glacierised Himalayan catchments. *Hydrology and Earth System Sciences.* [preprint], https://doi.org/10.5194/hess-2021-499.

Li, L., Shen, M., Hou, Y. et al. (2019). Twenty-first-century glacio-hydrological changes in the Himalayan headwater Beas River basin. *Hydrology and Earth System Sciences,* 23, 1483-1503.

NAO: National Weather Service – Climate Prediction Center, National Oceanic and Atmospheric Administration. (nd). *North Atlantic Oscillation (NAO).* https://www.cpc.ncep.noaa.gov/products/precip/CWlink/pna/nao.shtml.

NINO indices: IRI Data Library by Lamont Doherty Earth Observatory, Columbia University. (nd). *Indices nino EXTENDED.* http://iridl.ldeo.columbia.edu/SOURCES/.Indices/.nino/.EXTENDED/?Set-Language=en&sem=iridl%3AClimate-Indices.

PDO: National Centers for Environmental Information, National Oceanic and Atmospheric Administration. (nd). *Pacific Decadal Oscillation (PDO).* https://www.ncdc.noaa.gov/teleconnections/pdo/.

Peings, Y., Douville, H., Colin, J. Saint Martin, D. and Magnusdottir, G. (2017). Snow-(N)AO Teleconnection and its modulation by the quasi-biennial oscillation, *Journal of Climate*, 30(24), 10211-10235.

QBO index: IRI Data Library by Lamont Doherty Earth Observatory, Columbia University. (nd). *Indices QBO.* https://iridl.ldeo.columbia.edu/SOURCES/.Indices/.QBO/index.html?Set-Language=en.

River Discharge: Harrigan, S., Zsoter, E., Barnard, C., Wetterhall, F., Ferrario, I., Mazzetti, C., Alfieri, L., Salamon, P., Prudhomme, C. (2021). River discharge and related historical data from the Global Flood Awareness System, v3.1. *Copernicus Climate Change Service (C3S) Climate Data Store (CDS)*. https://cds.climate.copernicus.eu/cdsapp#!/dataset/cems-glofas-historical?tab=overview.

Shah, A., Sheeba, K., et al. (2018). Living With Earthquake and Flood Hazards in Jammu and Kashmir, NW Himalaya. *Frontiers in earth science,* 6.

Shaman, J. and Tziperman, E. (2005). The effect of ENSO on Tibetan Plateau snow depth: A stationary wave teleconnection mechanism and implications for the South Asian monsoons. *Journal of Climate*, 18(12), 2067-2079.

Sharma, S., Kuniyal, J.C (2016). Hydropower development and policies in India: A case of Himachal Pradesh in the northwestern Himalaya, India. *Energy Sources, Part B: Economics, Planning, and Policy,* 11(4), 377-384

Singh, J., Yadav, R.R. and Wilmking, M. (2009). A 694-year tree-ring based rainfall reconstruction from Himachal Pradesh, India. *Climate Dynamics,* 33, 1149-1158.

SOI: Global Climate Observing System - Working Group on Surface Pressure. (nd). *Southern Oscillation Index (SOI).* https://psl.noaa.gov/gcos_wgsp/Timeseries/SOI/.

